ELSEVIER

Nuclear Physics A 673 (2000) 64–84

NUCLEAR PHYSICS A

www.elsevier.nl/locate/npe

The rotational γ-continuum in the mass region $A \approx 110$

A. Bracco [a], S. Frattini [a], S. Leoni [a], F. Camera [a], B. Million [a], N. Blasi [a], G. Falconi [a], G. Lo Bianco [a], M. Pignanelli [a], E. Vigezzi [a], B. Herskind [b], M. Bergström [b], P. Varmette [b], S. Törmänen [b], A. Maj [c], M. Kmiecik [c], D.R. Napoli [d], M. Matsuo [e]

[a] *Dipartimento di Fisica, Universitá di Milano, and INFN sez. Milano, via Celoria 16, 20133 Milano, Italy*
[b] *The Niels Bohr Institute, Copenhagen, Denmark*
[c] *The Henryk Niewodniczański Institute of Nuclear Physics, 31-342 Kraków, Poland*
[d] *INFN, Laboratori Nazionali di Legnaro, Legnaro, Italy*
[e] *Yukawa Institute for Theoretical Physics, Kyoto, Japan*

Received 27 January 2000; revised 14 February 2000; accepted 15 February 2000

Abstract

Unresolved γ transitions of ^{114}Te and of ^{112}Sn sorted into one-dimensional and two-dimensional spectra have been studied. The reaction ^{64}Ni + ^{54}Cr at bombarding energies 230, 240, 250, 260, 270 MeV was used and the γ-rays were detected with the EUROBALL array. In the case of the nucleus ^{114}Te the values of the multiplicity as a function of bombarding energy and of the moment of inertia were obtained. The effective moment of inertia was found to be almost constant in the interval $I = 20$–$40\ \hbar$, in contrast to the decreasing behaviour of the dynamic moment of inertia for the terminating yrast band. The ridge valley structures in $E_{\gamma_1} \times E_{\gamma_2}$ spectra of ^{114}Te and of ^{112}Sn were analysed with the fluctuation analysis technique. The analysis of the two nuclei are compared to simulations based on microscopic cranking calculations with residual interactions included. A rather good agreement is found between data and predictions.

PACS: 21.10.Tg; 21.10.Re; 21.60.Ka; 23.20.En; 23.20.Lv

1. Introduction

In the last few years several efforts have been made to study the properties of the rotational motion in thermally excited nuclei. The important mechanism characterizing the nuclear structure in this regime is the progressive mixing of rotational bands with increasing excitation energy, together with the onset of the damping of rotational motion. The emission of unresolved γ-transitions with energy E_γ up to approximately 2 MeV is

0375-9474/00/$ – see front matter
PII: S0375-9474(00)00149-4

an experimental feature of the damped rotational motion and consequently the study of continuous spectra gives important insights into this problem.

Until now, the most extensive experimental and theoretical work on the damping of rotational motion has been made for nuclei in the mass region $A \approx 160$, characterized by rather stable nuclear deformation up to high thermal energy [1]. The overall features of quasi-continuum spectra have been well described with the rotational damping model based on cranked shell model plus residual interaction calculations [2,3]. The microscopic calculations predict a large variation of the rotational damping as a function of deformation, mass number and nuclear species. This variation was already predicted and discussed in the original formulation of the rotational damping model [4]. In that work schematic estimates for the scaling with mass number were derived. In particular, the bording energy U_0 at which the damping sets in, depending on the level density and on the strength of the residual interaction, is predicted to vary with mass number, $U_0 \propto A^{-2/3}$. In addition, the rotational damping width $\Gamma_{\rm rot}$, expressing the width of the quadrupole transition strength distribution, is proportional to the statistical dispersion of the rotational frequency of cranked shell model n particle–n hole states. For $\Gamma_{\rm rot}$ the scaling is expected to follow the relation $\Gamma_{\rm rot} \propto I A^{-5/2} \varepsilon^{-1}$, where I, A, and ε are the spin, mass number and deformation, respectively. According to this expression the damping width of a nucleus with mass number $A \approx 110$ is expected to be a factor of approximately two larger than that of a nucleus with $A \approx 160$, provided the two nuclei have similar deformations.

In a recent letter, a comparative study of one- (1D) and two-dimensional (2D) unresolved quasi-continuum spectra of ^{114}Te and ^{164}Yb nuclei was reported [5]. Overall, the comparison has shown consistency in the scaling of the rotational damping width with mass number, as predicted by the original schematic damping model. In this connection, it is important to remark that while several nuclei with $A \approx 160$ have already been investigated, ^{114}Te is the first nucleus in the mass region $A \approx 110$ studied with the same analysis techniques earlier developed for rare earth nuclei. It is therefore interesting to investigate the quasi-continuum in other nuclei of the mass region $A \approx 110$, to verify the conclusion obtained in the ^{114}Te case [5].

For this reason we have extended the previous investigation of the rotational damping properties in the mass region $A \approx 110$, where the rotational properties of the low lying discrete bands have been extensively studied in a number of different nuclei [6–10]. In particular, we have focused our attention on the nucleus ^{112}Sn, which was populated as a residue with comparable intensity by the reaction used for the study of ^{114}Te. The present paper is therefore intended to report on the comparative study of 1D and 2D quasi-continuum spectra of the ^{112}Sn and ^{114}Te nuclei, in terms of excitation function, effective moment of inertia, lifetimes and fluctuations of counts in γ–γ coincidence matrices. The comparison of the results for these two nuclei, expected to have similar properties at high spins, provides further support to the previous conclusions concerning the mass dependence of rotational damping, giving also a more consistent picture of the thermal rotation in the $A \approx 110$ mass region. In addition, a detailed description of the main features of the simulation calculations used to compare the experimental results to theory is given in the appendix of the paper.

2. The experiment

The experiment was performed at the Legnaro National Laboratory (Italy) using beams from the Tandem Accelerator. The fusion reaction $^{64}\mathrm{Ni} + {}^{54}\mathrm{Cr} \Rightarrow {}^{118}\mathrm{Te}$ at bombarding energies $E_{\mathrm{beam}} = 230$, 240, 250, 260 and 270 MeV was used. The γ-rays were detected by the EUROBALL array [11], consisting of 13 Ge cluster detectors, 25 Ge clover detectors and 28 tapered detectors. Data were obtained for a self supporting thin target with a thickness of 550 μg/cm^2 and for a target 400 μg/cm^2 thick on a Au backing 50 mg/cm^2 thick. The initial velocity of the residual nuclei in the middle of the target was deduced to be $v/c = 4.6 \pm 0.2\%$ (the error giving the values corresponding to the lowest and highest bombarding energies). The calculated maximum angular momentum is 56, 61, 67, 71, and 74 $\hbar$, for the bombarding energies 230, 240, 250, 260 and 270 MeV, respectively. Energy-dependent time gates on the Ge time signal were used to suppress background from neutrons. The largest fraction of the data was obtained at the bombarding energy of 250 MeV both with thin and backed target. At this bombarding energy the two strongest channels, populated with approximately the same intensity ($\approx 20\%$), were the $4n$ and $\alpha 2n$ leading to the ^{114}Te and ^{112}Sn residual nuclei, respectively, as deduced from the counts in the transition from the first excited state to the ground state. Previous discrete spectroscopy works on these two nuclei have shown a complex spherical level scheme structure at low spin, while long sequences of rotational intruder bands have been observed to develop up to spin 50 $\hbar$ in the ^{114}Te case [7,8]. In addition, one of the earliest investigations of continuum γ-rays in the low energy region $0 < E_\gamma < 4$ MeV made by NaI detectors showed, in the case of the reaction $^{82}\mathrm{Se} + {}^{40}\mathrm{Ar} \Rightarrow {}^{122}\mathrm{Te}$, the presence of a bump of quadrupole nature, peaking at ≈ 1.8 MeV and increasing in intensity with the projectile bombarding energy. This has suggested a possible rotational-like behaviour setting in at rather high spins ($\approx 35\ \hbar$), when the residual nuclei populated by this reaction develop a permanent deformation [12].

In the following sections of the paper we present a more detailed investigation of the quasi-continuum in $A \approx 110$ mass region focussing on the two nuclei ^{114}Te and ^{112}Sn for which 1D and 2D γ-coincidence spectra were measured with high efficiency Ge detectors.

3. Analysis of the spectra

Unresolved γ transitions deexciting the warm rotating nucleus above the yrast line form quasi-continuum structures in both 1D and 2D spectra. In particular, a pronounced continuous bump of quadrupole character, superposed on an exponential distribution of statistical E1 nature, is usually observed in 1D spectra in the energy region where discrete transitions are weak, and do not dominate the spectrum strongly ($E_\gamma \geqslant 1$ MeV for rare earth nuclei). The analysis of such distribution can provide valuable information on the average properties of the rotational motion in the damped regime, like for example the effective moment of inertia and the lifetimes of the transitions populating the continuous bump. In Sections 3.1–3.4 the techniques extensively used to analyze this quasi-continuum

structure observed in 1D spectra of rare earth nuclei are described in connection with their application for the analysis of the measured one-dimensional spectra associated with the ^{114}Te and ^{112}Sn nuclei.

More detailed information on the rotational properties of the warm nucleus can be obtained by the analysis of γ–γ coincidence matrices. In fact, while discrete rotational bands of low excitation energy produce ridge structures parallel to the main diagonal $E_{\gamma_1} \approx E_{\gamma_2}$, damped transitions spread out more uniformly, filling also the $E_{\gamma_1} \approx E_{\gamma_2}$ valley region. The ridge-valley features present in 2D rotational spectra have been extensively studied in the case of rare earth nuclei to extract quantitative information on the two different regimes of rotational motion. In Section 3.5, 2D spectra gated on ^{114}Te and ^{112}Sn nuclei will be studied, making use in particular of a statistical analysis technique of the count fluctuations of γ–γ coincidence spectra [13] earlier applied to nuclei of the $A \approx 160$ mass region. The experimental results will be also compared to cranked shell model calculations including a two body residual interaction.

3.1. Excitation function

One way to determine the rotational nature of the unresolved γ transitions forming a continuous bump in one-dimensional spectra is to compare spectra measured at different beam energies (excitation function). In fact, because the spin-energy distribution of compound nuclei formed by fusion reaction moves to higher values of both angular momentum and excitation energy with increasing bombarding energies also the associated residual nuclei should be formed at higher spin and thermal energy. Therefore, for a given residual nucleus, to an increase in bombarding energy should correspond the emission of additional rotational transitions at higher spins characterized by higher γ-ray energies. This gives rise to an increase of both the intensity and the average transition energy of the continuous bump observed in 1D spectra.

In Fig. 1 the one-dimensional spectra measured for ^{114}Te and ^{112}Sn at bombarding energies of 230, 240, 250, 260 and 270 MeV are shown, after background subtraction and correction for the detector efficiency. The transitions used as gates to select the ^{114}Te and ^{112}Sn nuclei are listed in Table 1, respectively.

The spectra have been corrected for the detection efficiency and normalized to the number of counts associated with the measured average multiplicity (see Section 3.2) at each bombarding energy. In addition to the data, a dashed line is shown in Fig. 1, representing the E1 contribution to the spectrum. This E1 statistical component has been obtained by fitting the 1D spectra in the transition energy region 2.8–3.5 MeV, by the exponential function $\approx E_\gamma^3 \exp(-E_\gamma/T)$, being $T \approx 0.6$ MeV the nuclear temperature.

One can clearly note for both nuclei the presence of a pronounced continuous bump in the transition energy region $\geqslant 1.4$ MeV of increasing intensity up to a bombarding energy of 260 MeV. At the bombarding energy of 270 MeV the measured yield does not further increase being equal to the spectrum taken at 260 MeV. These facts support the rotational nature of the continuous bump. One expects to see an energy increase of the rotational bump only up to transition energies corresponding to the maximum value of the angular

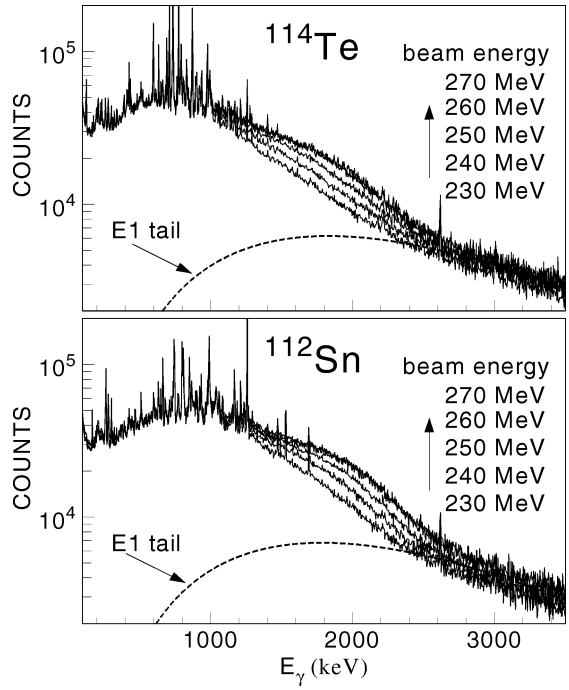

Fig. 1. The one-dimensional γ-ray spectra measured at different bombarding energies in coincidence with low spin transitions of ^{114}Te and ^{112}Sn are shown in the top and bottom panels, respectively. The spectra, background subtracted and corrected for the detector efficiency, are normalized to the number of counts associated with the measured average multiplicity (see Section 3.2). The arrows indicate that the spectra with the lowest number of counts in the continuous distribution correspond to the lowest bombarding energy. The dashed lines represent the E1 contribution to the spectra, parametrized as described in the text.

Table 1
Transitions used as gates to sort 1D and 2D spectra of ^{114}Te and ^{112}Sn

^{114}Te	^{112}Sn
709 keV ($2^+ \rightarrow 0^+$)	630 keV ($6^+ \rightarrow 4^+$)
775 keV ($4^+ \rightarrow 2^+$)	663 keV ($8^+ \rightarrow 6^+$)
734 keV ($6^+ \rightarrow 4^+$)	263 keV ($9^- \rightarrow 8^-$)
871 keV ($8^+ \rightarrow 6^+$)	741 keV ($10^+ \rightarrow 8^+$)

momentum that the nucleus can sustain. In the present case one observes that at 260 MeV the limit is reached, implying that the additional 10 MeV only pump more energy into the compound nucleus, without giving any more spin to the system. One can also note that the characteristic transition energy of the measured bump is $\approx$ 1.8–2 MeV, which is higher than that measured for a typical rare earth nucleus ($\approx$ 1.2–1.3 MeV). This is consistent

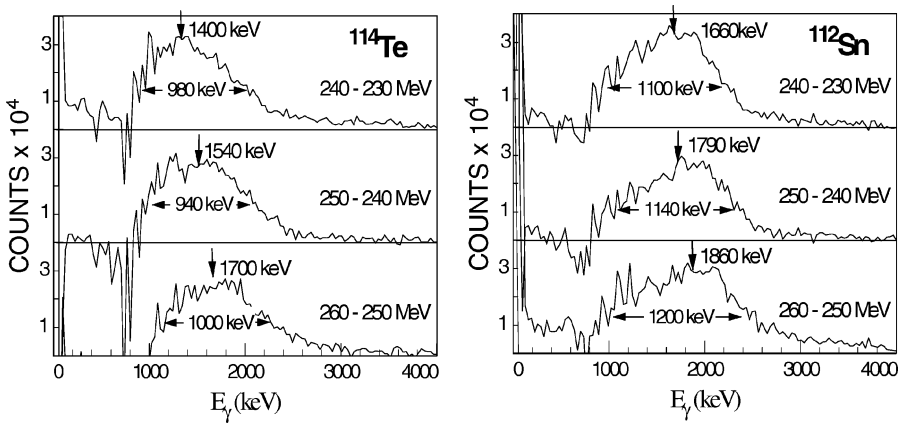

Fig. 2. The spectra obtained as difference between two consecutive bombarding energies are shown for ^{114}Te in the left panel and for ^{112}Sn in the right panel. The vertical arrows indicate the position of the centroid of the distribution and the horizontal arrows the width of the distribution.

with the fact that at a given spin the rotational transition energy is higher for a nucleus with smaller value of the moment of inertia, being $E_\gamma \propto \Im^{-1} \propto A^{-5/3}$.

The spectral shape distribution of the additional γ-rays emitted when the bombarding energy is increased can be obtained as a difference between spectra corresponding to two consecutive incident energies. Figure 2 shows the measured distribution obtained in the case of ^{114}Te and ^{112}Sn nuclei starting from the spectra shown in Fig. 1. In both cases one can see that the difference spectra form a continuous bump with a centroid moving towards higher energy with increasing spin (bombarding energy), supporting the rotational character of the transitions present in the bump. The difference spectra are in fact expected to contain mostly the high spin transitions emitted at the residual nucleus entry level. In addition, the average transition energy of the continuous bump is found to be higher in the case of ^{112}Sn. There could be two different explanations for this. The first is that each residue, being populated by the emission of different types of particles, is populated with a different spin-energy distribution. In particular, the ^{112}Sn nucleus, corresponding to the emission of one α and two neutrons could be populated at higher spins, consistently with the fact that α emission can compete with fission. The second explanation can be related to the fact that the ^{112}Sn nucleus has a moment of inertia slightly smaller than that of ^{114}Te (of the order of 15%), implying higher transition energies. In this connection it is important to anticipate part of the results presented in Section 4, in which the analysis of the ridge-valley structure in $E_{\gamma_1} \times E_{\gamma_2}$ spectra is discussed. In fact, as it will be shown, the moment of inertia obtained from the position of the first ridge in ^{112}Sn corresponds to a value which is $\approx$ 15–20% smaller than that of ^{114}Te. However, since the ridge structure probes an excitation energy region lower than that of the continuum bump, one can not completely exclude, by the ridge analysis only, changes in the effective moment of inertia at higher spins (or γ transition energies). Unfortunately, as it will be discussed in Section 3.5, it was not possible in the case of ^{112}Sn to measure directly the effective moment of inertia of the bump, which would give a more definite answer to this point.

The widths of the distribution of the difference spectra shown in Fig. 2 are expected in principle to reflect the width of the rotational damping $\Gamma_{\rm rot}$. However it is not possible to determine $\Gamma_{\rm rot}$ from the width of these spectra because they do not contain the E2 transitions corresponding to a given $I \rightarrow I - 2$ decay only. In contrast, all the decays from an entry spin distribution contribute to the difference spectrum so that its width can only give an upper limit for $\Gamma_{\rm rot}$. In the present case, the width of the distribution of the difference spectra has values around 1 MeV in the case of the ^{114}Te nucleus. Instead values slightly higher (up to 1200 keV) are found for ^{112}Sn and this could be a consequence of a possible population of this nucleus at higher spins. In general, the present values are approximately two times larger than those measured for rare earth nuclei [5]. The scaling with mass number of the rotational damping width, discussed in Ref. [5] in connection with the ^{114}Te nucleus only, is therefore confirmed by the additional data on ^{112}Sn.

3.2. Average γ-ray multiplicity of ^{114}Te

The average multiplicity $\langle M_\gamma \rangle$ of γ-rays has been extracted from the ^{114}Te 1D spectra measured at different bombarding energies and shown in Fig. 1. In general, this quantity can be deduced by dividing the total number of counts in the spectrum by the intensity of the lowest spin transition collecting the entire decay flow of the nucleus, representing multiplicity 1. In the case of a gated spectrum, one would need two consecutive transitions collecting the complete γ-flow (the lowest for the gate on the residue and the other for the multiplicity normalization), as for example the $4^+ \rightarrow 2^+ \rightarrow 0^+$ transitions in ^{114}Te.

In the case of ^{112}Sn this procedure could not be applied due to the complex level scheme at low spin, which does not allow to select two clean consecutive transitions collecting the entire decay flow. However, one can be confident, even without knowing the absolute value of $\langle M_\gamma \rangle$ in the specific case of ^{112}Sn, that the increase in the average multiplicity from one beam energy to the next is approximately the same as in the ^{114}Te case.

In Fig. 3 the experimental values of $\langle M_\gamma \rangle$ obtained from the analysis of the 1D spectra of ^{114}Te at the different bombarding energies are shown. From the average multiplicity $\langle M_\gamma \rangle$ one can determine the average initial spin of the residual nucleus, assuming a given number of E1 statistical transitions in each cascade ($\approx$ 2–3). From Fig. 3 one can see that the

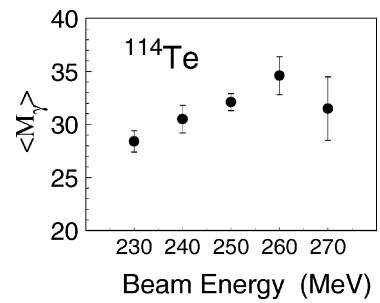

Fig. 3. Average γ multiplicity corresponding to the ^{114}Te nucleus measured at the different bombarding energies.

difference in multiplicity ΔM_γ between two consecutive beam energies is approximately constant and equal to 2. This means that in average one gets two additional stretched E2 transitions, corresponding to an increase in spin of 4 units when the beam energy is increased by 10 MeV. Calculations of the kinematic of the reaction also predict an increase of the average spin of the same order (4–5 $\hbar$).

Before discussing the present results for the relative increase of γ-ray average multiplicity of ^{114}Te and their connection with the displacement of the average γ-ray energy measured in the difference spectra, it is important to recall the relevant feature of the cold rotation in this nucleus at high spin, namely that of the band termination [7]. In fact, the moment of inertia associated with of the near yrast bands was found to decrease smoothly with increasing spin, indicating that the collective rotation terminates (smooth band termination [6], seen also in other nuclei of the same mass region). At higher internal energy the band termination phenomenon might not be present because the larger number of available microscopic configurations can result in a collective rotation also at the highest spins. Two extreme and different situations, namely one assuming a constant moment of inertia equal to that measured at low spin and the other assuming the smooth band termination behaviour were therefore considered and the corresponding spin increases associated with the measured displacement of the average γ energy in the difference spectra were determined. As discussed below, only in one case consistency is found between the measurement of the increase in the average γ multiplicity and the displacement of the average γ-ray energy in the difference spectra.

In Fig. 4 the filled triangles show the relation between γ-transition energy and spin for the 3 measured discrete bands [7] (the γ transition energies were averaged over the 3 bands for each given spin). One can note that around $I = 34\,\hbar$ there is a change of slope, when the band termination effect sets in. The horizontal dashed lines indicate the position of the

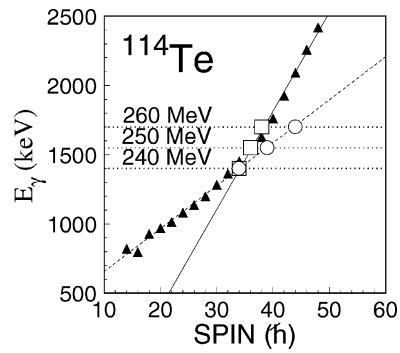

Fig. 4. The average γ-transition energies of the measured discrete transitions are shown as function of spin by filled triangles. The dashed line is a fit to the low spin region ($I < 34\,\hbar$), before band termination occurs, while the solid line is a fit to the high spin data in the band termination region ($I > 34\,\hbar$). The horizontal dotted lines correspond to the centroid of the distributions of the difference spectra reported in Fig. 2. The crossings of the horizontal lines with the full drawn lines are shown by open squares, while the crossings with the dashed lines are shown by open circles (see text for discussion).

measured average γ-ray energy of the continuous bump present in the difference spectra (cf. Figs. 2(a), (b) and (c)). Two straight lines are also shown, their slope representing the inverse of the moment of inertia. The dashed line is the fit to the low spin region $I < 34\,\hbar$, before band termination occurs, while the full drawn line is the fit to the data in the band termination region $I > 34\,\hbar$. The crossings of the horizontal lines with the full drawn line (band terminating moment of inertia) are shown by open squares, while the crossing with the dashed lines (low spin moment of inertia) are shown by open circles. If one assumes for the moment of inertia associated with the continuous bump the same value seen at high spin in the discrete bands (band termination), the corresponding spin increase is ≈ 2 units. In contrast, an increase of 4 units is found if one assumes that the moment of inertia of the excited nucleus at $I \geqslant 30\,\hbar$ is similar to that at lower spins. This last point is supported not only by the measured value of the increase in multiplicity (shown in Fig. 3 and consistent with the kinematics), but also by the results obtained for the effective moment of inertia of the continuous bump, as it will be discussed in detail in the next section.

Based on the fact that only by assuming for the damped transitions the same moment of inertia measured at $I \leqslant 30\,\hbar$ it is possible to find a consistency between the measured value of the average γ-ray energy in different spectra and the measured increase in the average total γ-ray multiplicity, we can conclude that the band termination effects does not seem to be a general property of the rotational damped transitions.

3.3. *Effective moment of inertia*

For a rotational like cascade it is possible, also in the case of continuous γ-transitions, to estimate the value of the effective moment of inertia of the rotating nucleus. The effective moment of inertia $\Im^{(2)}_{\text{eff}}$ can be obtained from the height of the continuous bump in 1D spectra [14,15]. The method used is based on the fact that, if the damped transitions follow in average the main properties of the nuclear collective rotation, their energies can be related to the average first and second moment of inertia $\Im^{(1)}_{\text{eff}}$ and $\Im^{(2)}_{\text{eff}}$ by the same relations satisfied by the discrete transitions, namely $\langle E_\gamma \rangle = 2\hbar I/\Im^{(1)}_{\text{eff}}$ and $\Delta E_\gamma = \langle E_{\gamma_1} - E_{\gamma 2} \rangle = 4\hbar/\Im^{(2)}_{\text{eff}}$. This implies that for a given number of E2 transitions the bump will be more compressed (being ΔE_γ smaller) if $\Im^{(2)}_{\text{eff}}$ is large, and more stretched out if $\Im^{(2)}_{\text{eff}}$ is small. As a consequence, the height $H(E_\gamma)$ of a 1D quasi-continuum spectrum, after subtracting the E1 statistical component and normalizing the total area to the absolute multiplicity of the rotational cascades, can be related to the effective moment of inertia $\Im^{(2)}_{\text{eff}}$ by the relation [14,15]

$$\frac{H(E_\gamma)}{f(E_\gamma)} = \frac{dN}{dE_\gamma} = \frac{\Im^{(2)}_{\text{eff}}}{4\hbar^2}. \tag{1}$$

Here, dN/dE_γ is the number of counts per unit interval, and $f(E_\gamma)$ is the feeding function, i.e., the fraction of observed population which goes through a γ-ray energy interval.

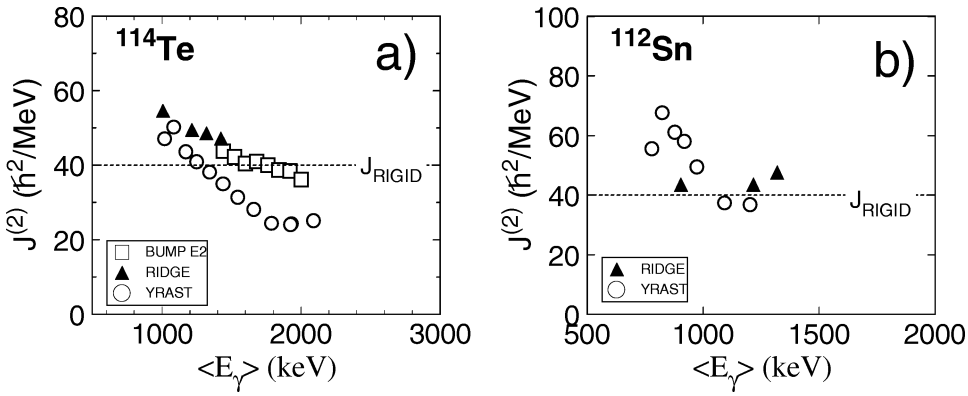

Fig. 5. The dynamical moment of inertia $\Im^{(2)}_{\rm eff}$ for ^{114}Te (a) and ^{112}Sn (b). The open circles correspond to the discrete transitions, the filled triangles to the ridges and the open squares to the continuous bump. The horizontal dashed lines give the moment of inertia of the rigid rotor.

The feeding function $f(E_\gamma)$, which is given by [14,15]

$$f(E_\gamma) = \left[\int_{E_\gamma}^{\infty} \Delta S(E_\gamma)\, dE_\gamma\right] \Big/ \left[\int_{0}^{\infty} \Delta S(E_\gamma)\, dE_\gamma\right],$$

has been obtained using as ΔS the difference of spectra measured at two different bombarding energies.

The results for the effective moment of inertia $\Im^{(2)}_{\rm eff}$ of ^{114}Te are shown in Fig. 5(a) (open squares) together with the averaged values obtained from the discrete transitions (open circles) of the known rotational bands [7]. In contrast with the behaviour of the near yrast bands, the dynamical moment of inertia of the damped transitions of the continuous bump is nearly constant and has a value very close to that of the rigid rotor (shown in Fig. 5(a) with the dashed line). This result is in agreement with the analysis of the average multiplicity $\langle M_\gamma \rangle$ reported in the previous section and could point to the absence of a band termination effect for the thermally excited rotational states of ^{114}Te. However, since what we measure is an effective moment of inertia, which reflects the net effect of the superposition of different excited bands having a spread in the value of the moment of inertia, one cannot completely rule out the presence of some excited bands with similar behaviour of the measured discrete bands.

In the case of ^{112}Sn, due to the difficulty in determining experimentally the value of $\langle M_\gamma \rangle$, which is needed to obtain an absolute normalization of the 1D spectrum, a similar analysis could not be performed (see discussion in Section 3.2).

3.4. Lifetimes

Another evidence of the collective character of the quasi-continuum bump can be obtained from lifetime measurements of the γ-decay. In the case of the present experiment we applied the DSAM technique for measuring the fractional Doppler shifts to the data taken with the Au backed target.

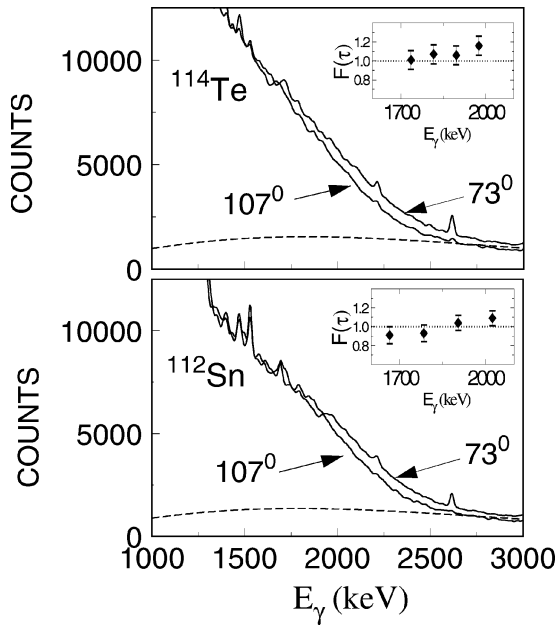

Fig. 6. The one-dimensional spectra measured at 73° and 107° for ^{114}Te are shown in the top panel and those of ^{112}Sn in the bottom panel. The dashed lines represent the E1 statistical component, calculated as discussed in Section 3.1. The insets give the values of the obtained fractional Doppler shifts.

In order to compare spectra with the same response function, which make more reliable the estimate of the Doppler shift of the continuous bump, we have not used the entire data set, but only the data obtained with the clover Ge detectors [11]. This was possible, in spite of the small difference in angle at which the clover detectors are positioned, because of the high value of the v/c ($\approx 4.6\%$) of the recoiling nuclei emitting the γ-rays. The spectra corresponding to 73° and 107° corrected for the detector efficiency, are shown in Fig. 6 for ^{114}Te and ^{112}Sn, respectively. In both cases shifts in the region of the damped transitions are clearly visible. The corresponding values of the fractional shifts were obtained as described below. The fractional shift is given by $F(\tau) = \Delta E_\gamma / \Delta E_\gamma^{\max}$, being $\Delta E_\gamma = E_\gamma (v/c)\cos(\theta)$ and $\Delta E_\gamma^{\max}$ the shift corresponding to the initial velocity $v_{\max}$ of the recoil.

It has been assumed that the spectrum in a small interval around each point in the region of the continuous bump can be approximated by a straight line [16,17],

$$N(E_\gamma) = dN/dE_\gamma \times E_\gamma + c. \tag{2}$$

Consequently, for the spectra at forward (F) and backward (B) angles one has:

$$N_{F(B)}(E_\gamma) = dN/dE_\gamma \times (E_\gamma \pm \Delta E_\gamma) + c. \tag{3}$$

Because in the interval 1600–2000 keV the slope dN/dE_γ varies very slowly with E_γ, one can assume that $dN/dE_\gamma(E_\gamma + \Delta E_\gamma) \approx dN/dE_\gamma(E_\gamma - \Delta E_\gamma)$, so that the difference between the forward and backward spectra is $\Delta N = dN/dE_\gamma \times 2\Delta E_\gamma(E_\gamma)$. In order

to extract the shifts $\Delta E_\gamma(E_\gamma)$, the term dN/dE_γ has to be eliminated. For this purpose an average spectrum $N^{\rm av}(E_\gamma)$ was obtained from the sum of the forward and backward spectra. Two shifted spectra were then created starting from $N^{\rm av}(E_\gamma)$, namely:

$$N^{\rm av}_{F(B)}(E_\gamma) = dN/dE_\gamma \times (E_\gamma \pm (\Delta E_\gamma)_{\rm max}) + c, \tag{4}$$

where $(\Delta E_\gamma)_{\rm max}$ is the Doppler shift corresponding to the maximum velocity of the recoiling γ-emitting nucleus. In practice, the shift $(\Delta E_\gamma)_{\rm max}$ used to construct the shifted spectra $N^{\rm av}_{F(B)}$ was taken constant and calculated at the reference energy $E_{\gamma_0} = 2.8$ MeV, corresponding to fully shifted transitions. In this way the maximum Doppler shift at the energy E_γ can be related to the Doppler shift at E_{γ_0} by the relation

$$(\Delta E_\gamma)_{\rm max}(E_\gamma) = (\Delta E_\gamma)_{\rm max}(E_{\gamma_0}) \times \frac{E_\gamma}{E_{\gamma_0}}. \tag{5}$$

The fractional shift can then be deduced as the ratio between the difference spectra:

$$F(\tau, E_\gamma) = \frac{\Delta E_\gamma(E_\gamma)}{(\Delta E_\gamma)_{\rm max}(E_\gamma)} = \frac{N_{73^\circ}(E_\gamma) - N_{107^\circ}(E_\gamma)}{N^{\rm av}_F(E_\gamma) - N^{\rm av}_B(E_\gamma)} \times \frac{E_{\gamma_0}}{E_\gamma}. \tag{6}$$

The fractional shifts obtained with the above procedure are shown in the insets of Fig. 6. For both ^{114}Te and ^{112}Sn nuclei the analysis was made in the region of the lower edge of the continuous bump, namely for the transition energy region $1.7 < E_\gamma < 2$ MeV, where the continuous bump strongly dominates over the E1 statistical component, shown by dashed lines in the figure. The values are found to be consistent with fully shifted transitions and consequently we can only set an upper limit of $\approx 10^{-14}$ s for the effective feeding-times plus lifetime of the E2 damped transitions. Although it is not possible to deduce the nuclear deformation for the damped rotations one can note that this limit is consistent with collective type of rotation.

3.5. Analysis of 2D spectra

A better identification of the rotational pattern for unresolved transitions can be achieved examining the $E_{\gamma_1} \times E_{\gamma_2}$ coincidence spectra [13]. In fact, as it has been clearly seen in the case of rare earth nuclei, unresolved transitions of regular rotational bands form a ridge structure, while damped transitions from mixed rotational bands fill the $E_{\gamma_1} \approx E_{\gamma_2}$ valley region. The data associated to the ^{114}Te and ^{112}Sn nuclei were sorted into γ–γ coincidence spectra gated by the same low lying transitions used for the one-dimensional analysis, and given in Table 1. Two-dimensional spectra of uncorrelated events for background subtraction purposes were also constructed using the raw data and the UNCOR technique described in Ref. [18]. The $E_{\gamma_1} \times E_{\gamma_2}$ spectra, obtained after subtraction of uncorrelated events and removal of the contribution of known intense discrete transitions [19] (denoted by COR spectra) were then used for further analysis. In panels (a) and (b) of Fig. 7 two perpendicular cuts, 100 keV wide, at the average transition energy $(E_{\gamma_1} + E_{\gamma_2})/2 = 1200$ and 1400 keV projected onto the axis $E_{\gamma_1} - E_{\gamma_2}$ are displayed for the ^{114}Te nucleus, while in panels (c) and (d) two cuts at the average energies $(E_{\gamma_1} + E_{\gamma_2})/2 = 1200$ and 1300 keV, respectively, are displayed for the ^{112}Sn nucleus. A ridge-valley structure can

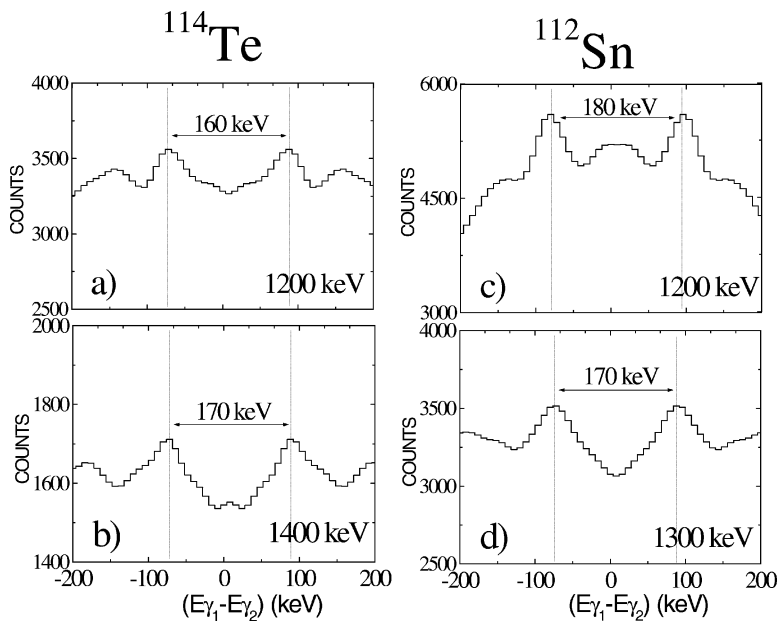

Fig. 7. Examples of perpendicular cuts on the $E_{\gamma_1} \times E_{\gamma_2}$ matrices for ^{114}Te (left column) and ^{112}Sn (right column) for two different values of the average γ transition energy $(E_{\gamma_1} + E_{\gamma_2})/2$. The distance between the two inner most ridges, being equal to $2\times 4\hbar^2/\Im^{(2)}$, is indicated by the arrows.

be seen for both ^{114}Te and ^{112}Sn, although the feature is in general less pronounced than in the case of rare earth nuclei (see, for example, Ref. [5]). The intensity of the ridge structure is rather weak, of the order of 3% and very similar to that found for the three resolved rotational bands (cf. Fig. 12). In addition, the separation among the first ridges is found to be $\approx$ 160–180 keV, which is larger than the typical values of rare earth nuclei ($\approx$ 120 keV), as expected from the rotation of a nucleus with smaller moment of inertia. The relation for two rotational γ-transitions $E_{\gamma_1} - E_{\gamma_2} = \pm 4/\Im^{(2)}$ was used to obtain the values of the dynamical moment of inertia from the position of the first ridges. The corresponding results are shown with the triangles in Figs. 5(a) and 5(b) in comparison with the values obtained from the discrete transitions. In the case of ^{114}Te the value of the effective dynamical moment of inertia obtained from the analysis of the ridges and of the continuous one-dimensional bump show all together a much smaller decrease with average γ-transition energy (spin) as compared to the discrete bands, and their values are very close to that of the rigid rotor. Values similar to the rigid rotor were found also in the case of the ridge analysis of ^{112}Sn, although for this nucleus the information is restricted to a smaller interval of average γ-transition energy.

The $E_{\gamma_1} \times E_{\gamma_2}$ spectrum was analysed in the ridge-valley region using the fluctuation analysis technique [13]. The method has been developed to extract quantitative information from the quasi-continuum spectra to be compared to model predictions. The main idea behind the method is based on the fact that, in the course of the decay, the nucleus can select among a finite number of pairs of γ-transitions $(E_{\gamma_1}, E_{\gamma_2})$ leading to a given sector

of the plane ($E_{\gamma_1} \times E_{\gamma_2}$). This finiteness leads to fluctuations superimposed to ordinary statistical fluctuations in the number of counts. In particular, the number of paths that the nucleus has available in its decay can be obtained from the data. The expression $N^{(2)}_{\text{path}} = \frac{N_{\text{eve}}}{\mu_2/\mu_1 - 1}$ is used, where μ_1 and μ_2 are the first and the second moment of the number of counts and N_{eve} is the number of events in the selected sector (chosen to be a square of $4/\Im \times 4/\Im$ keV^2) along the valley or along the ridges. The width of the sector used for this analysis was 100 keV $\times$ 100 keV. The values of μ_1 and μ_2 were obtained using the program STATFIT [13].

Because of the complex level scheme having a number of high energy transitions at low spin, care had to be taken to select for the fluctuation analysis only the cuts not contaminated by the presence of such γ-transitions. Therefore the number of clean cuts for which the fluctuation analysis could be applied is rather limited. Although the study of higher-dimensional correlations is expected to emphasize even better the rotational structures, it was not possible with the statistics of the present experiment to study higher-order correlations. The number of paths deduced from the ^{114}Te and ^{112}Sn data is rather similar, both in the ridge and in the valley region, as one can see in Figs. 8(a) and (b) where the experimental findings are shown.

For the first ridge the number of paths measured for the two nuclei is in both cases of the order of 10 and approximately 2.5 times smaller than that obtained for nuclei in the $A \approx 160$ mass region. To illustrate this point in Fig. 8 we have shown also the results

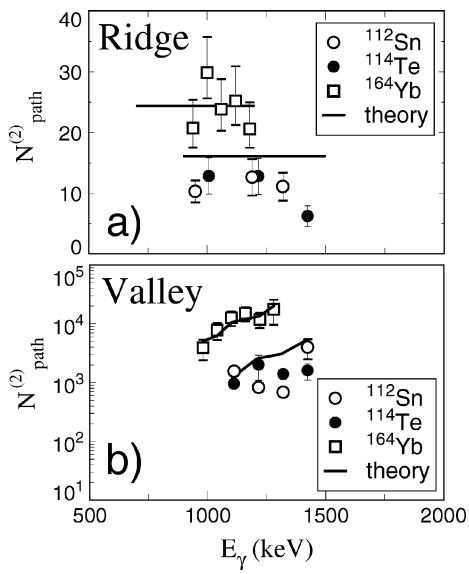

Fig. 8. Top part: The effective number of paths $N^{(2)}_{\text{path}}$, extracted from the first ridge analysis of the measured spectra for ^{114}Te, ^{112}Sn and ^{164}Yb. The full drawn lines correspond to the number of discrete bands predicted by the theory (satisfying the condition $n_{\text{branch}} \leqslant 2$), averaged over the spin region 25–35 $\hbar$. Bottom part: The quantity $N^{(2)}_{\text{path}}$ extracted from the valley analysis for ^{114}Te, ^{112}Sn and ^{164}Yb. The curves are the corresponding values predicted by the theory.

reported in reference [5] for the nucleus ^{164}Yb. The number of paths in the first ridge gives approximately the number of regular discrete bands [13] having at least two consecutive γ-transitions before damping sets in, as a consequence of the high level density and of the mixing due to the residual interaction. The number of discrete bands can be directly obtained from the theoretical calculations by counting the number of two consecutive transitions having the property that the corresponding branching number n_{branch} is less or equal to 2 [2]. The value of n_{branch} gives a measure of the fragmentation of the E2 strength. It is defined as $n_{\text{branch}}(i) = (\sum_j b_{i,j}^2)^{-1}$, where $b_{i,j}$ is the normalized strength from level i at spin I to level j at spin $I-2$. Using n_{branch} it is also possible to deduce the onset energy U_0 for rotational damping, energy corresponding to $n_{\text{branch}} = 2$. In the case of ^{114}Te the onset energy U_0 is approximately 1.4 MeV at $I > 30\ \hbar$, while it is approximately 0.8–1 MeV for rare earth nuclei as a consequence of their higher density of levels.

The values of N_{path} obtained for the band mixing calculations on ^{114}Te [2], averaged over the spin interval 25–35 $\hbar$, are shown by the full drawn line in Fig. 8(a) in comparison with the experimental values. The theory is found to reproduce rather well the experimental values of N_{path} for the rotational motion in this mass region.

The number of paths obtained from the analysis of the valley region, collecting mostly damped transitions from states at which one expects the fragmentation of the rotational decay, are shown in Fig. 8(b). Also in this case very similar results (of the order of 10^3) are found for the ^{114}Te and ^{112}Sn data. The values measured in this mass region are approximately one order of magnitude smaller than those measured for rare earth nuclei, as one can see from the data relative to ^{164}Yb also shown in the figure. The expected values of N_{path} for the valley region depend on the value of the rotational damping width but also, more strongly, on the value of the level density. It is important to recall that the rotational damping width predicted by the calculation is in the case of $A = 110$ nuclei a factor of two larger than that of $A = 160$ nuclei, while the level density is smaller. Therefore, the comparison with the theory requires the derivation of the same quantity N_{path} from a simulated spectrum calculated using the microscopic excited levels and transition probabilities (cf., e.g., [20]). The spectra for ^{114}Te were constructed using the same cranked shell model calculation plus a surface delta residual interaction mixing the mean field rotational bands [2] used for the ridge analysis discussed above. The description of the simulation procedure and of the relevant features of the microscopically calculated quantities entering in the simulation calculation are reported in the appendix.

The results for N_{path} obtained applying the fluctuation technique to the simulated spectra in the valley region are shown in Fig. 8(b) with the full drawn line. The agreement between the data and the predictions for the ^{114}Te nucleus is rather satisfactory, although one can note that the general trend of the theory is that of overpredicting the data, both for the ridge and valley cases in particular for the ^{112}Sn nucleus. The mass dependence of the N_{path} quantity in the ridge and valley regions is well reproduced by the same model as one can see from the comparison with the ^{164}Yb results also shown in Fig. 8, although improvements for the calculations for the mass region $A \approx 110$ and more data are desirable.

4. Conclusion

A study of the properties of the quasi-continuum in the mass region $A \approx 110$ was here discussed, focussing on the nuclei ^{114}Te and ^{112}Sn at high spins. One-dimensional and two-dimensional gated spectra were analysed.

The continuous bump present in one-dimensional spectra was first studied as a function of bombarding energies and its fractional Doppler shift was deduced using the DSAM technique. Evidence for collective type of rotation was found. In the case of ^{114}Te also the effective dynamical moment of inertia was obtained and values very close to the rigid body were found. This is in contrast to the smooth decrease observed in the moment of inertia of the resolved discrete bands characterized by the band termination effect.

Ridge-valley structures have been identified for both nuclei in the two-dimensional $E_{\gamma_1} \times E_{\gamma_2}$ spectra. The fluctuation analysis was applied and very similar results were obtained for the two nuclei, which are different from those of the $A \approx 160$ mass region. A comparison with the model predictions has been made using simulation based on microscopic calculations of the band mixing process by the residual interaction.

Altogether, the fact that similar experimental results were found for two nuclei gives a stronger support to the mass dependence predicted by the rotational damping model. However, more selective data from higher order correlations are desirable to have a further and better test of the rotational band mixing in the $A \approx 110$ mass region.

5. Appendix: Simulations with band mixing calculations

In the case of the study of the rotational continuum in rare earth nuclei, simulations based on microscopically calculated levels have been shown to be very useful to sharpen the comparison between theory and experiments. To make use of the power of the fluctuation analysis method for the study of the quasi-continuum one needs to obtain the values of N_{path} also from the theory. In the case of the ridge one can obtain the value of N_{path} by simply counting the number of two consecutive transitions having a $B(\text{E2})$ which does not branch to more than two levels, as discussed in Section 3.5. In the case of the valley the situation is more complicated and the quantity N_{path} cannot be simply obtained from the calculations, since it strongly depends on the decay flow of the excited rotating nucleus. For this reason one needs to construct simulated spectra of the same type as the experimental data to be analyzed with the statistical methods [20].

Microscopic cranked shell model calculations have been made for ^{114}Te by Matsuo et al. [2], producing individual nuclear levels and E2 transition probabilities extending up in the region where the damping of the rotational motion is dominant. In the model the single particle basis is obtained cranking the particle–hole states of a Nilsson potential (with parameter $\beta = 0.25$, $\gamma = 0°$), representing the intrinsic excitations of the rotational nucleus. Each np–nh configuration forms a rotational band. The rotational bands are mixed by a two-body residual interaction of surface delta type with standard interaction strength $V_0 = 27.5\ \text{MeV}/A$ [21].

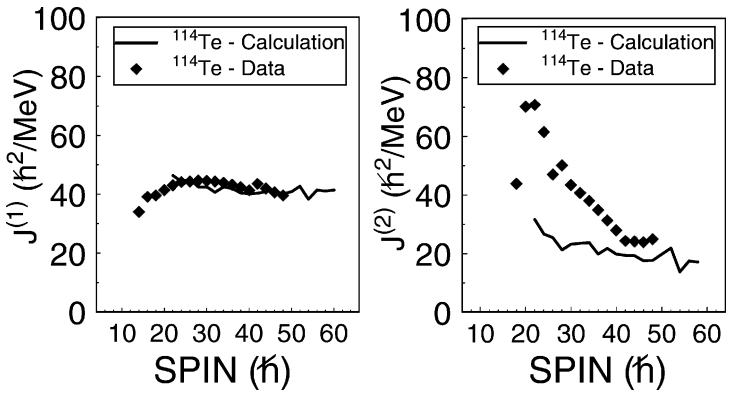

Fig. 9. The average kinematic moment of inertia $\Im^{(1)}$ of the regular discrete bands having $n_{\text{branch}} \leqslant 2$, as obtained from the band mixing calculation, is shown in comparison with the data in the left panel. A comparison of the same type is shown in the right panel for the average dynamical moment of inertia $\Im^{(2)}$.

It is interesting to discuss the main features of the physical quantities entering into the simulation, namely the kinematic and dynamic moment of inertia of the rotational bands, the B(E1) and B(E2) strength and the level density. The average values of the kinematic and dynamic moment of inertia are shown in Fig. 9 for the calculated discrete rotational bands having $n_{\text{branch}} < 2$, in comparison with the experimental values. While in the case of the kinematic moment of inertia $\Im^{(1)}$ the calculated values are very similar to that of the discrete bands in the whole spin range the same is not true in the case of the dynamic moment of inertia $\Im^{(2)}$. The latter is much smaller than the experimental values obtained for the discrete bands, also in the spin region interval 30 to 40 $\hbar$, region in which the experimental study of the continuum in 1D and 2D spectra was made. However, for the purpose we are interested in, which is mainly the number of paths in the valley region, this disagreement should not be a major drawback. In fact, the value of the dynamic moment of inertia $\Im^{(2)}$ affects only the position of the ridges and it is not expected to affect the results concerning the central valley which is well separated by the ridge structures. Also the value of n_{branch}, used to calculate the number of discrete rotational bands, is mainly controlled by the strength of the residual interaction and by the level density and should not be strongly affected by the value of $\Im^{(2)}$.

The main feature of the model prediction relevant for the study of the continuum is the variation of the E2 rotational strength distribution with spin I and internal energy U. In Fig. 10 a number of B(E2) strength distributions for ^{114}Te are shown corresponding to spin 30 and 46 $\hbar$. They are obtained using the branching factors $b(E_i, E_f)$ of each transition from level i to all possible final levels f (quantities directly used by the simulation code for the E2 transition at each decay step) and then averaging over the energy intervals 0–1, 1–1.5, 1.5–2.0, 2.0–2.5 and 2.5–3.5 MeV (from the top to the bottom panels). As one can see, the mean value of these distributions does not depend on the internal energy U, but only on the spin I as expected for the typical γ-transitions among levels of rotational bands satisfying the relation $E_\gamma = 2I/\Im^{(1)}$. In contrast, the width and the shape of the

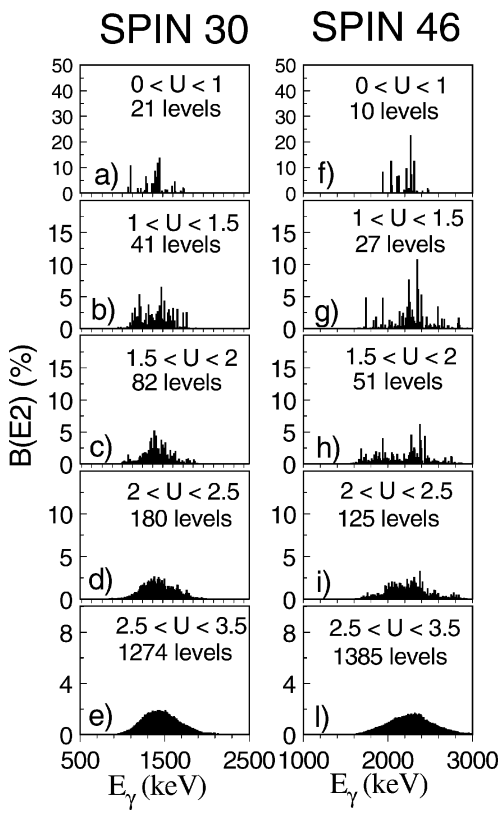

Fig. 10. The B(E2) strength distributions for ^{114}Te corresponding to spin 30 and 46 $\hbar$ are shown in the left and right panels, respectively. They were obtained averaging over the energy intervals 0–1, 1–1.5, 1.5–2.0, 2.0–2.5 and 2.5–3.5 MeV (from the top to the bottom panels).

B(E2) distribution are strongly affected by U. At high internal energy the distribution is rather smooth and wide as a consequence of the strong mixing of close lying states due to the residual interaction.

In the schematic rotational damping model [4], the width of the B(E2) strength, which coincides with the rotational damping width $\Gamma_{\rm rot}$, is directly related to the spreading of the rotational frequency $\Delta\omega$ of the different unperturbed rotational bands, being $\Gamma_{\rm rot} = 2\Delta\omega$. In Fig. 11 values of $2\Delta\omega$ deduced from the transition energies of the cranked shell model bands are plotted for two selected spin values as a function of the internal energy U. From here one can notice that rather large values of $\Gamma_{\rm rot}$ are predicted for this nucleus, reaching values of the order of 0.5 MeV.

The level density $\rho(U)$ of the calculated nuclear states has been obtained by fitting the levels with the function:

$$\rho(U) = \frac{\sqrt{\pi}}{48}\frac{\exp 2\sqrt{aU}}{a^{1/4}U^{5/4}}. \tag{7}$$

The expression of the level density is used to calculate the E1 transition probability

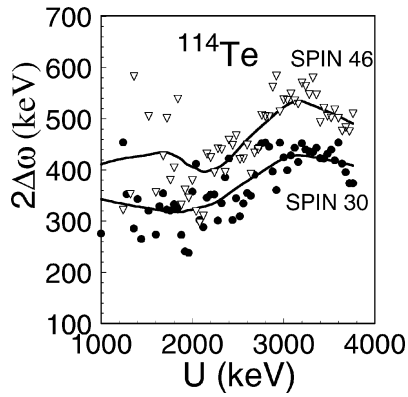

Fig. 11. The spreading $2\Delta\omega$ of the rotational frequency of the cranked shell model bands is plotted for two selected spin values as a function of the internal energy U, averaging over 40 keV bins. The lines correspond to a smooth interpolation of the points. As discussed in the text, the width of the B(E2) strength, giving directly the rotational damping width $\Gamma_{\rm rot}$, is found in good agreement with the relation $\Gamma_{\rm rot} = 2\Delta\omega$ [4].

$$T(\mathrm{E1}, U_i) = H_{\mathrm{E1}} \int_0^{U_i} (U_i - U)^3 f_{\mathrm{GDR}}(U_i - U) \frac{\rho(U)}{\rho(U_i)}\, dU. \tag{8}$$

Here the strength function f_{GDR} is given by the tail of the giant dipole resonance (GDR), of Lorentzian shape with centroid $E_0 = 15$ MeV and width $\Gamma_{\mathrm{E1}} = 5$ MeV. As in the case of the rare earth nuclei [20] we have found that one has to reduce substantially the value of f_{GDR}, as compared to the value deduced assuming that the GDR exhausts the E1 sum rule, in order to reproduce the average experimental intensity of low-lying bands. This is in agreement with previous studies [22]. The associated hindrance factor is denoted H_{E1} in Eq. (8). In the region of discrete levels, the integral in expression (8) is replaced by a summation. The resulting population of the lowest states is displayed in Fig. 12. This quantity is affected by the competition between statistical and rotational transitions [23], which in turn also determine the asymptotic behaviour of $\langle U(I)\rangle$. In the present simulation this competition is controlled by the hindrance factor H_{E1}, adjusted to 0.01 in order to have an overall agreement between the measured and simulated intensities.

In Fig. 13 we show three cuts of a simulated 2D matrix at average transition energy $(E_{\gamma_1} + E_{\gamma_2})/2 = 1100$, 1300 and 1500 keV. One can notice a ridge-valley structure similar to the one observed in the experimental data (cf. Fig. 7), although the distance between the inner ridges appear to be larger, as a consequence of the lower values of the calculated moment of inertia $\Im^{(2)}$ as compared with the experimental ones. These simulated spectra were used to perform the fluctuation analysis of the ridge-valley structure, whose results are discussed in Section 3.5 in comparison with the experimental data.

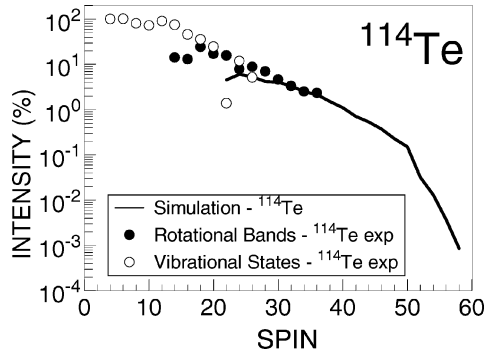

Fig. 12. The measured intensity of the discrete γ-transitions of ^{114}Te is shown by circles. The line shows the intensity obtained in the simulated spectra for the yrast transitions.

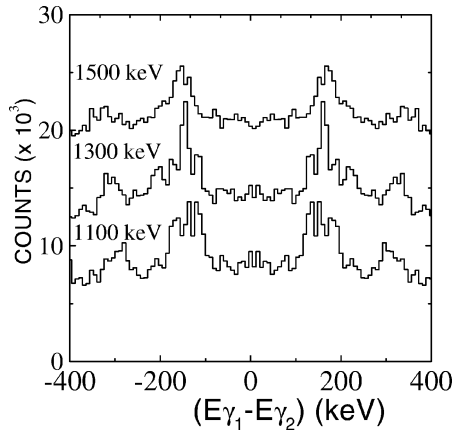

Fig. 13. Examples of perpendicular cuts on the $E_{\gamma_1} \times E_{\gamma_2}$ simulated matrices for ^{114}Te corresponding to three different values of the average γ transition energy $(E_{\gamma_1} + E_{\gamma_2})/2$.

Acknowledgement

The work has been supported by the Italian Istituto Nazionale di Fisica Nucleare and the Danish Natural Science Research Council and the Polish Committee for Scientific Research (KBN, grant no. 2 P03 B001 16).

References

[1] S. Frattini, A. Bracco, S. Leoni, P. Bosetti, B. Herskind, T. Døssing, M. Bergström, G.B. Hagemann, H. Ryde, J.P. Vivien, A. Bagshow, D. Smalley, A.G. Smith, Phys. Rev. Lett. 81 (1998) 2659.
[2] M. Matsuo, T. Døssing, E. Vigezzi, R.A. Broglia, K. Yoshida, Nucl. Phys. A 617 (1997) 1.
[3] M. Matsuo, K. Yoshida, T. Døssing, E. Vigezzi, R.A. Broglia, Nucl. Phys. A 649 (1999) 379c.
[4] B. Lauritzen, T. Døssing, R.A. Broglia, Nucl. Phys. A 457 (1986) 61.

[5] S. Frattini, A. Bracco, S. Leoni, F. Camera, B. Million, N. Blasi, G. Lo Bianco, M. Pignanelli, E. Vigezzi, B. Herskind, T. Døssing, M. Bergström, P. Varmette, S. Törmänen, A. Maj, K. Kmiecik, D.R. Napoli, M. Matsuo, Phys. Rev. Lett. 83 (1999) 5234.
[6] A.V. Afanasjev, D.B. Fossan, G.J. Lane, I. Ragnarsson, Phys. Rep. 322 (1999) 1.
[7] I. Thorslund, D. Fossan, D.R. LaFosse, H. Schnare, K. Hauschild, I.M. Hibbert, S.M. Mullins, E.S. Pauls, I. Ragnarsson, J.M. Sears, P. Vaska, R. Wadsworth, Phys. Rev. C 52 (1995) R2839.
[8] H. Harada, T. Murakami, K. Yoshida, J. Kasagi, T. Inamura, T. Kubo, Phys. Lett. B 207 (1988).
[9] R. Wadsworth, H.R. Andrews, C.W. Beausang, R.M. Clark, J. DeGraaf, D.B. Fossan, A. Galindo-Uribarri, I.M. Hibbert, K. Hauschild, J.R. Huges, V.P. Janzen, D.R. LaFosse, S.M. Mullins, E.S. Paul, L. Persson, S. Pilotte, D.C. Radford, H. Schnare, P. Vaska, D. Ward, J.N. Wilson, I. Ragnarsson, Phys. Rev. C 50 (1994) 483.
[10] J.M. Sears, D.B. Fossan, I. Thorslund, P. Vaska, E.S. Paul, K. Hauschild, I.M. Hibbert, R. Wadsworth, S.M. Mullins, A.V. Afanasjev, I. Ragnarsson, Phys. Rev. C 55 (1997) 2290.
[11] J. Simpson, Heavy Ion Physics 6 (1997) 253.
[12] M.A. Deleplanque, Th. Byrski, R.M. Diamond, H. Hübel, F. Stephens, B. Herskind, R. Bauer, Phys. Rev. Lett. 41 (1978) 1105.
[13] T. Døssing, B. Herskind, S. Leoni, A. Bracco, R.A. Broglia, M. Matsuo, E. Vigezzi, Phys. Rep. 268 (1) (1996) 1.
[14] F.S. Stephens, Phys. Scr. T 5 (1983) 5.
[15] M.A. Deleplanque, H.J. Körner, H. Kluge, A.O. Macchiavelli, N. Bendjaballah, R.M. Diamond, F.S. Stephens, Phys. Rev. Lett. 50 (1983) 409.
[16] H. Hübel, U. Smilansky, R.M. Diamond, F.S. Stephens, B. Herskind, Phys. Rev. Lett. 41 (1978) 791.
[17] B. Million, S. Leoni, A. Bracco, J. Moretti, S. Frattini, P. Bosetti, F. Camera, M. Mattiuzzi, B. Herskind, R.A. Bark, I. Bearden, G.B. Hagemann, H.J. Jensen, Phys. Lett. B 415 (1997) 321.
[18] O. Andersen, J.D. Garrett, G.B. Hagemann, B. Herskind, D.L. Hillis, L.L. Riedinger, Phys. Rev. Lett. 43 (1979) 10.
[19] D.C. Radford, Nucl. Inst. Meth. A 361 (1995) 297.
[20] A. Bracco, P. Bosetti, S. Frattini, E. Vigezzi, S. Leoni, T. Døssing, B. Herskind, M. Matsuo, Phys. Rev. Lett. 76 (1996) 4484.
[21] A. Faessler, Fortschr. Phys. 16 (1968) 309.
[22] G. Leander, Phys. Rev. C 38 (1988) 728.
[23] T. Døssing, E. Vigezzi, Nucl. Phys. A 587 (1995) 13.